Linking Changes in Sulcal Morphometry to Cognitive Development from Childhood to Adolescence

Supplemental Information

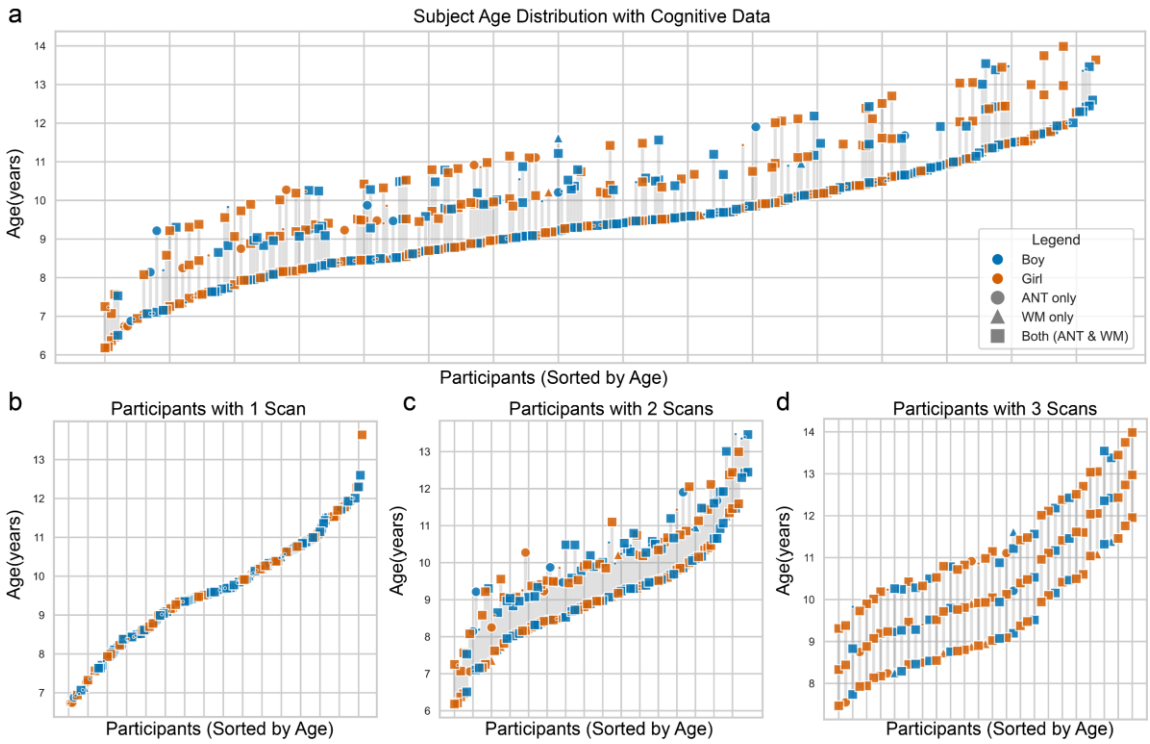

Supplementary Figure 1. Age distribution of participants and cognitive data availability.

The x-axis represents individual participants sorted by their baseline age, with gray lines connecting repeated scans of the same individual. Colors denote gender (blue for boys; orange for girls). Different marker shapes indicate the availability of cognitive data at each specific time point, including data from the Attention Network Test (ANT) and/or Working Memory (WM; N-back task). (a) Full sample distribution: Age distribution for the entire longitudinal dataset (n = 490 scans from 312 participants). (b–d) Sub-group distributions: Separate panels for participants with (b) one scan, (c) two scans, and (d) three or more scans.

Following data quality control, we utilized a longitudinal sMRI dataset composed of 312 typically developing children aged 6.1 to 13.9 years (F/M = 145/167) from the Childhood Brain Development Project (CBD, Beijing cohort). Among these children, some underwent repeated MRI scans every year, resulting in a total of 490 MRI scans. Specifically, 47 children (F/M = 31/16) had three available scans, 97 children (F/M = 49/48) had two available scans, and 168 children (F/M = 65/103) had one available scan. All participants were recruited from elementary schools in Beijing and were confirmed to have normal cognitive abilities according to a well-validated standardized cognitive assessment in Mandarin[1]. Among them, 402 participants have WM data and 411 participants have ANT data.

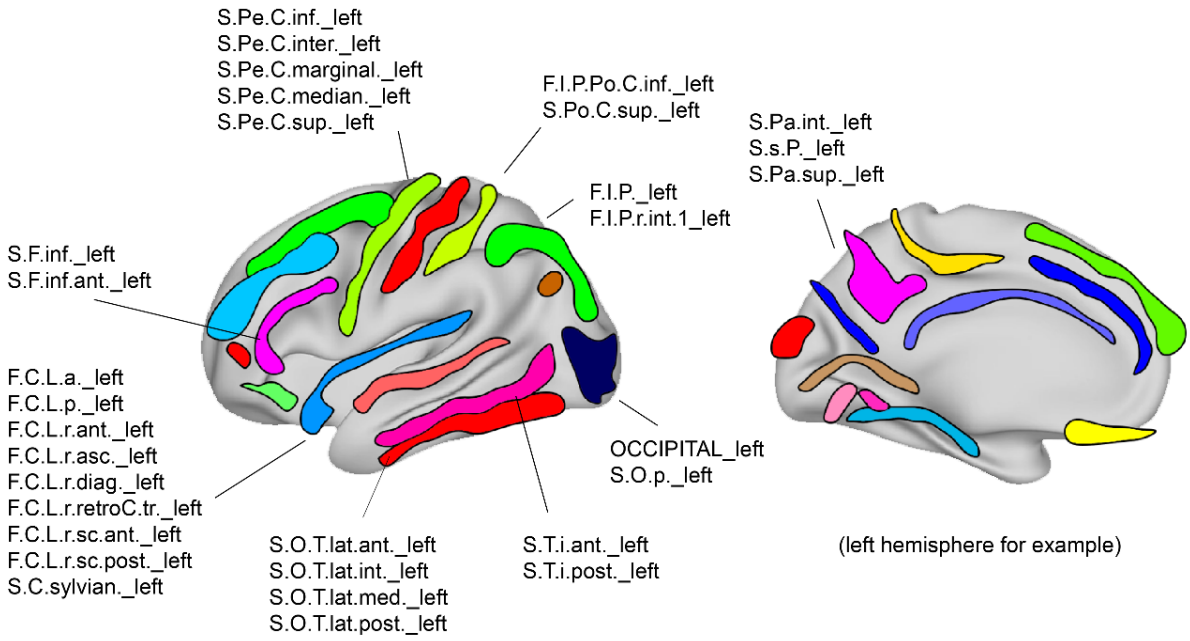

Supplementary Figure 2: Sulcal merging strategy

Following automatic segmentation by BrainVISA, sulci that were not successfully identified were manually filtered out through visual inspection. For the remaining sulci, fragmented or small segments of specific sulci (i.e., S.F.inf., F.C.L., S.O.T.lat., F.I.P., S.Po.C., S.Pe.C., S.T.i.) were merged into their complete anatomical units. Additionally, regions exhibiting significant inter-individual variability in their segmentation were combined into larger, cohesive anatomical units (e.g., OCCIPITAL, S.Pa.int.). Subsequent to these steps, the extraction success rate for all sulci was re-evaluated, leading to the exclusion of any sulci with a success rate below 75% (refer to Supplementary Figure 3 for details).

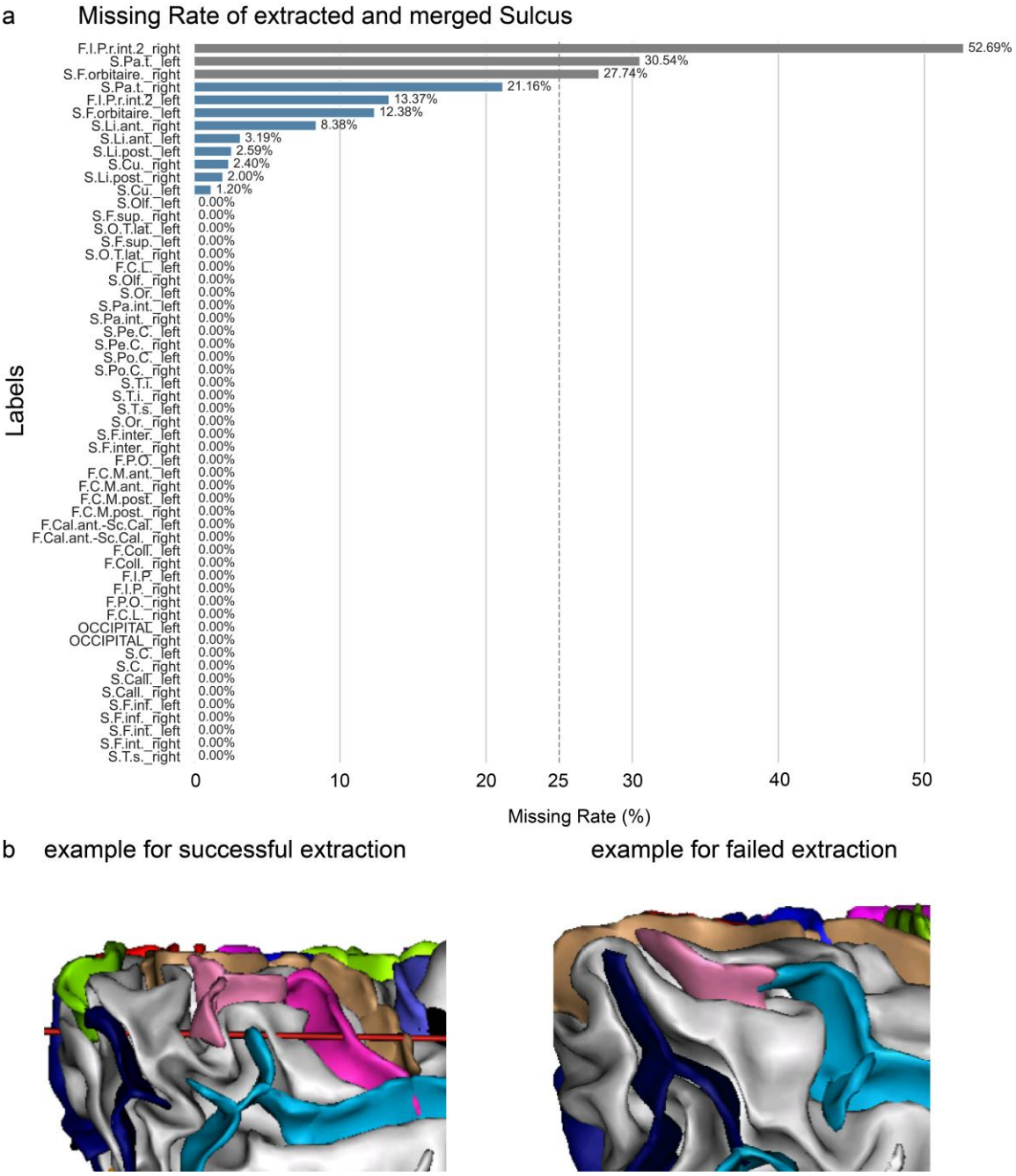

Supplementary Figure 3. Data quality control for automated sulcal extraction.
(a) Sulcal Extraction Missing Rates. Sulcal identification was performed across the cohort; the three specific sulci depicted with grey bars were excluded from subsequent analyses due to an extraction success rate below 75% (equivalent to a missing/error rate exceeding 25%). **(b)** Representative Examples of Sulcal Extraction. Visualization of successful (left) and failed (right) sulcal identification instances for the left anterior intralingual sulcus (Deep Pink), illustrating the criteria for quality control and anatomical inclusion.

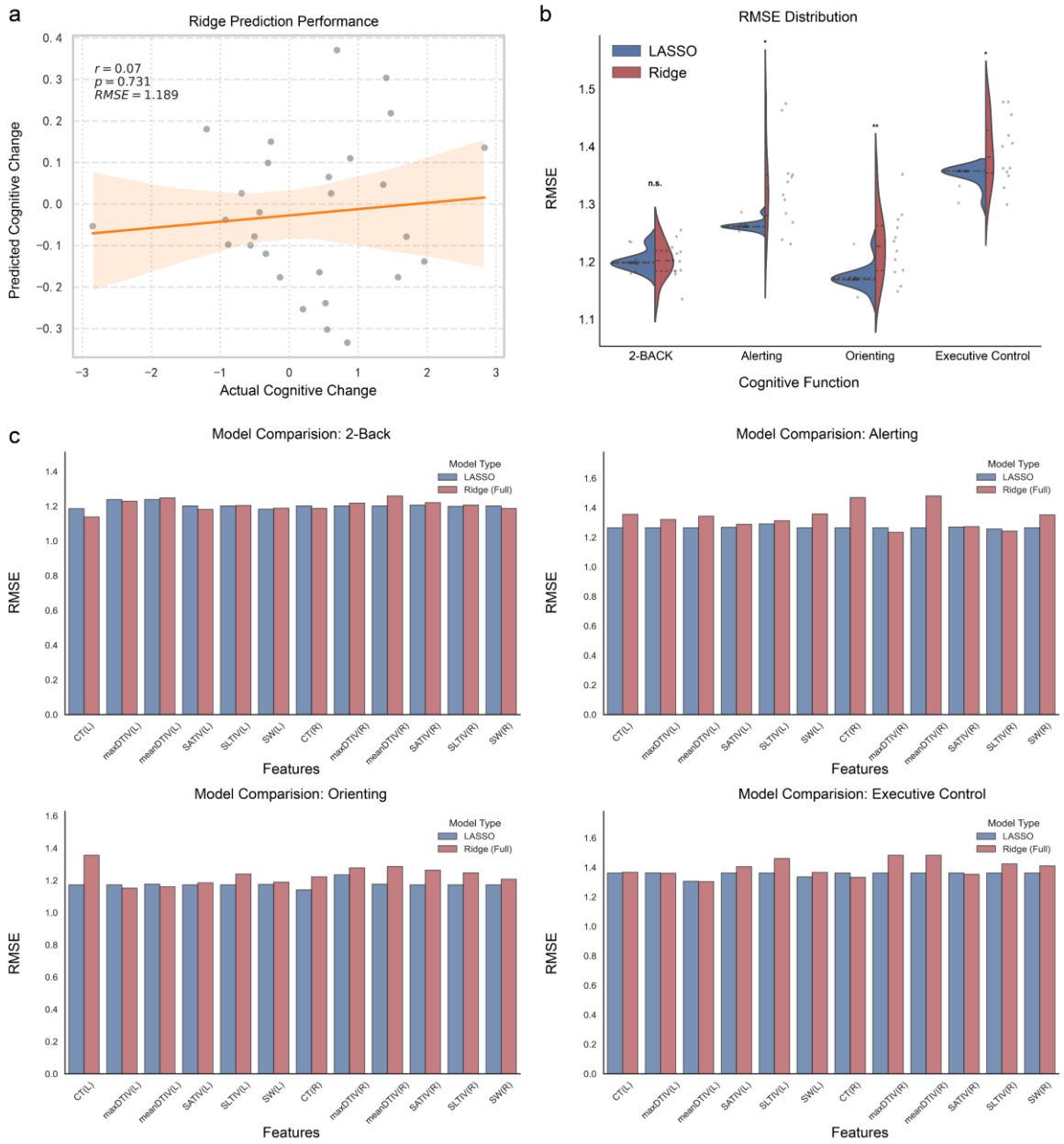

Supplementary Figure 4: Prediction Performance: Ridge vs. LASSO.
(a) Correlation between actual and predicted changes using the Ridge regression. All models were evaluated on an independent test set (20% of data). **(b)** Distribution of predictive errors (RMSE) across cognitive domains. Split-violin plots (organ plots) illustrate the distribution of Root Mean Square Error (RMSE) for the LASSO (feature-selected, blue) and Ridge (full-model, red) regression models across four cognitive functions: Working Memory (2-Back), Attention-Alerting, Attention-Orienting, and Attention-Executive Control. The horizontal dashed lines within the violins indicate the median and interquartile ranges, while individual data points (gray dots) represent specific brain structural indices. Statistical significance between the two models was determined using paired t-tests (*** $p < 0.001$, ** $p < 0.01$, * $p < 0.05$, n.s., not significant). **(c)** Comparison of predictive stability for specific brain features. Grouped bar charts display the RMSE for various sulcal morphometrics within each functional domain, separated by hemisphere (L: Left, R: Right). Lower RMSE values indicate higher predictive accuracy.

Supplementary Table 1. Definitions and emergence time of sulci in the present study

No.	Full Name	Label	Tapp[2–7]	T10[8]	T50[8]
1	Left lateral fissure	F.C.L._left	17.00	23.50	26.57
2	Right lateral fissure	F.C.L._right	17.00	23.50	26.61
3	Left calloso-marginal anterior fissure	F.C.M.ant._left	19.00	28.00	30.30
4	Right calloso-marginal anterior fissure	F.C.M.ant._right	19.00	28.00	30.40
5	Left calloso-marginal posterior fissure	F.C.M.post._left	19.00	27.10	29.26
6	Right calloso-marginal posterior fissure	F.C.M.post._right	19.00	27.20	29.42
7	Left calcarine fissure	F.Cal.ant.-Sc.Cal._left	16.00	24.80	27.61
8	Right calcarine fissure	F.Cal.ant.-Sc.Cal._right	16.00	24.70	27.70
9	Left collateral fissure	F.Coll._left	24.00	29.00	31.08
10	Right collateral fissure	F.Coll._right	24.00	28.90	31.39
11	Left intraparietal sulcus	F.I.P._left	29.00	28.10	30.31
12	Right intraparietal sulcus	F.I.P._right	29.00	28.20	30.45
13	Left secondary intermediate ramus of the intraparietal sulcus	F.I.P.r.int.2_left	38.00		
14	Left parieto-occipital fissure	F.P.O._left	17.00	25.80	29.36
15	Right parieto-occipital fissure	F.P.O._right	17.00	25.80	28.80
16	Left lobe occipital	OCCIPITAL_left	30.00	30.10	32.03
17	Right lobe occipital	OCCIPITAL_right	30.00	30.10	31.92
18	Left central sulcus	S.C._left	21.00	26.20	27.17
19	Right central sulcus	S.C._right	21.00	26.10	27.11
20	Left subcallosal sulcus	S.Call._left	28.00		
21	Right subcallosal sulcus	S.Call._right	28.00		
22	Left cuneal sulcus	S.Cu._left	16.00		
23	Right cuneal sulcus	S.Cu._right	16.00		
24	Left inferior frontal sulcus	S.F.inf._left	30.00	27.90	29.98
25	Right inferior frontal sulcus	S.F.inf._right	30.00	27.70	29.92
26	Left internal frontal sulcus	S.F.int._left	30.00	29.80	32.14
27	Right internal frontal sulcus	S.F.int._right	30.00	29.60	31.82
28	Left intermediate frontal sulcus	S.F.inter._left	30.00	29.20	31.61
29	Right intermediate frontal sulcus	S.F.inter._right	30.00	29.00	31.39
30	Left orbital frontal sulcus	S.F.orbitaire._left	33.00		
31	Left superior frontal sulcus	S.F.sup._left	30.00	29.10	30.72
32	Right superior frontal sulcus	S.F.sup._right	30.00	29.00	30.55
33	Left anterior intralingual sulcus	S.Li.ant._left			
34	Right anterior intralingual sulcus	S.Li.ant._right			
35	Left posterior intralingual sulcus	S.Li.post._left	35.00		
36	Right posterior intralingual sulcus	S.Li.post._right	35.00		
37	Left occipito-temporal lateral sulcus	S.O.T.lat._left	30.00	29.90	31.94
38	Right occipito-temporal lateral sulcus	S.O.T.lat._right	30.00	29.90	31.96
39	Left olfactory sulcus	S.Olf._left	17.00		
40	Right olfactory sulcus	S.Olf._right	17.00		
41	Left orbital sulcus	S.Or._left	22.00		

42	Right orbital sulcus	S.Or._right	22.00		
43	Left internal parietal sulcus	S.Pa.int._left			
44	Right internal parietal sulcus	S.Pa.int._right	29.00	28.70	31.98
45	Right transverse parietal sulcus	S.Pa.t._right	29.00	28.80	32.13
46	Left precentral sulcus	S.Pe.C._left	26.00	27.90	30.06
47	Right precentral sulcus	S.Pe.C._right	26.00	27.90	30.11
48	Left postcentral sulcus	S.Po.C._left	26.00	27.30	29.44
49	Right postcentral sulcus	S.Po.C._right	26.00	27.30	29.52
50	Left inferior temporal sulcus	S.T.i._left	31.00	29.40	32.45
51	Right inferior temporal sulcus	S.T.i._right	31.00	29.40	32.02
52	Left superior temporal sulcus	S.T.s._left	26.00	27.50	29.23
53	Right superior temporal sulcus	S.T.s._right	26.00	27.00	29.92

Supplementary Table 2. Sex Differences in Sulcal Morphometry.

Label	CT	maxD (adj)	meanD (adj)	SL (adj)	SW	SA (adj)
OCCIPITAL_left	2.24	0.36	0.56	1.08	**-3.71***	1.59
S.C._right	1.36	-0.74	-1.27	**3.32***	-2.8	2.46
S.F.inf._left	1.89	-0.99	-1.94	1.27	**-3.71***	-0.08
S.F.inf._right	0.08	-0.28	-0.4	1.29	**-3.54***	0.58
S.F.inter._left	0.32	0.99	0.57	0.25	**-3.42***	0.65
S.F.inter._right	2.1	0.77	0.03	0.84	**-3.91***	1
S.O.T.lat._right	0.29	2.12	1.88	1.12	**-3.43***	1.62
S.Pe.C._right	1.57	-0.77	0.66	0.71	**-3.74***	1.45
S.T.s._right	0.94	0.17	0.01	0.13	**-3.25***	0.62

Note: Values represent the T-statistics for the main effect of sex derived from the GAMMs. Positive values indicate significantly greater values in males compared to females, while negative values indicate greater values in females. Similar to the main analysis, Surface Area, Max Depth, and Mean Depth were adjusted for TIV.* indicate significant sex effects that survived FDR correction.

Abbreviations: adj: TIV-adjusted residuals; SA: Surface Area; maxD: Maximum Depth; meanD: Mean Depth; SW: Sulcal Width; CT: Cortical Thickness.

Supplementary Methods 1： Processing of Allen Human Brain Atlas Data

Regional microarray expression data were obtained from 6 post-mortem brains (1 female, ages 24.0–57.0, 42.50 ± 13.38) provided by the Allen Human Brain Atlas[9] (AHBA, https://human.brain-map.org). Data were processed with the abagen toolbox (version 0.1.3; https://github.com/rmarkello/abagen) using a 53-region volumetric atlas in MNI space. Microarray probes were first reannotated using updated gene annotations[10], with probes not matched to valid Entrez IDs being discarded. Probes were then filtered based on expression intensity relative to background noise [11], removing those with intensity below background in ≥50% of samples. When multiple probes indexed the same gene, the probe with the most consistent pattern of regional variation across donors was selected using differential stability measures[12].

Tissue sample MNI coordinates were updated using non-linear registration via Advanced Normalization Tools (ANTs), and samples were assigned to brain regions if located within 2 mm of atlas parcels. Sample-to-region matching was constrained by hemisphere and gross structural divisions to prevent misassignment[10]. Inter-subject variation was addressed by normalizing expression values using a robust sigmoid normalization function[13], followed by rescaling to the unit interval. Gene expression values were normalized across tissue samples using identical procedures, and samples assigned to the same brain region were averaged separately for each donor and then across donors, yielding the final regional expression matrix.

References

1. Fan, F. *et al.* Development of the default-mode network during childhood and adolescence: A longitudinal resting-state fMRI study. *NeuroImage* **226**, 117581 (2021).
2. Nishikuni, K. & Ribas, G. C. Study of fetal and postnatal morphological development of the brain sulci: Laboratory investigation. *Journal of Neurosurgery: Pediatrics* **11**, 1–11 (2013).
3. Chi, J. G., Dooling, E. C. & Gilles, F. H. Gyral development of the human brain. *Ann. Neurol.* **1**, 86–93 (1977).
4. Dubois, J. *et al.* Mapping the early cortical folding process in the preterm newborn brain. *Cerebral Cortex (New York, N.Y.: 1991)* **18**, 1444–1454 (2008).
5. Garel, C. *et al.* Fetal cerebral cortex: Normal gestational landmarks identified using prenatal MR imaging. *Ajnr Am. J. Neuroradiol.* **22**, 184–189 (2001).
6. Ono (M.D.), M., Kubik, S. & Abernathey, C. D. *Atlas of the Cerebral Sulci*. (Thieme, 1990).
7. Dubois, J. *et al.* The dynamics of cortical folding waves and prematurity-related deviations revealed by spatial and spectral analysis of gyrification. *NeuroImage* **185**, 934–946 (2019).
8. Snyder, W. E. *et al.* A bimodal taxonomy of adult human brain sulcal morphology related to timing of fetal sulcation and trans-sulcal gene expression gradients. *Neuron* **112**, 3396-3411.e6 (2024).
9. Hawrylycz, M. J. *et al.* An anatomically comprehensive atlas of the adult human brain transcriptome. *Nature* **489**, 391–399 (2012).
10. Arnatkevičiūtė, A., Fulcher, B. D. & Fornito, A. A practical guide to linking brain-wide

gene expression and neuroimaging data. *NeuroImage* **189**, 353–367 (2019).

11. Quackenbush, J. Microarray data normalization and transformation. *Nat Genet* **32**, 496–501 (2002).

12. Hawrylycz, M. *et al.* Canonical genetic signatures of the adult human brain. *Nat Neurosci* **18**, 1832–1844 (2015).

13. Fulcher, B. D., Little, M. A. & Jones, N. S. Highly comparative time-series analysis: The empirical structure of time series and their methods. *J. R. Soc. Interface* **10**, 20130048 (2013).